SCNNs: Spike-based Coupling Neural Networks for Understanding Structural-Functional Relationships in the Human Brain

Shaolong Wei[1†], **Shu Jiang**[1†], **Mingliang Wang**[2], **Liang Sun**[3], **Haonan Rao**[4], **Weiping Ding**[1] and **Jiashuang Huang**[1*]
[1]School of Artificial Intelligence and Computer Science, Nantong University, China
[2]School of Computer Science, Nanjing University of Information Science and Technology, China
[3]College of Artificial Intelligence, Nanjing University of Aeronautics and Astronautics, China
[4]School of Information Science and Technology, Nantong University, China
weishaolong37@gmail.com, jshmjs45@ntu.edu.cn, {wml489, sunl}@nuaa.edu.cn,
{haonanrao, dwp9988, hjshdym}@163.com

Abstract

Structural-functional coupling (SC-FC coupling) offers an effective approach for analyzing structural-functional relationships, capable of revealing the dependency of functional activity on the underlying white matter architecture. However, extant SC-FC coupling analysis methods primarily center on disclosing the statistical association between the topological patterns of structural connectivity (SC) and functional connectivity (FC), while often neglecting the neurobiological mechanisms by which the brain typically transmits and processes information in the form of spikes. To address this, we propose a biologically inspired deep-learning model called spike-based coupling neural networks (SCNNs). It can simulate spiking neural activity to more realistically reproduce the interaction between brain regions and the dynamic behavior of neuronal networks. Specifically, we first use spike neurons to capture the FC temporal characteristics of the original functional magnetic resonance imaging (fMRI) time series and the SC spatial characteristics of the structural brain network. Then, we use synaptic and neuronal filter effects to simulate the coupling mechanism of SC and FC in the brain at different temporal and spatial scales, thereby quantifying SC-FC coupling and providing support for the identification of brain diseases. The results on real datasets show that the proposed method can identify brain diseases and provide a new perspective for understanding SC-FC relationships.

1 Introduction

Analyzing the relationship between structure and function in the human brain is a current hot topic in neuroscience [Sporns, 2013]. Fundamentally, the brain's structure provides the physical basis for its complex functions, while functional changes may prompt structural adjustments in turn [Anderson and Finlay, 2014]. Most studies have indicated a close interconnection and synergy between the brain's regional structures and functions [Park and Friston, 2013; Pessoa, 2014; Petersen and Sporns, 2015]. In addition, the relationship between the local optimization function of the brain and the pattern of neuronal activity has prompted researchers to try to imitate the structure and function of the brain and develop artificial neural network models [Kanwisher *et al.*, 2023]. Therefore, in-depth research on the brain structure-function relationship aids in understanding brain complexity and provides crucial theoretical support for artificial intelligence.

Structural-functional brain connectivity coupling (SC-FC coupling) is a new paradigm for analyzing structural-functional relationships [Fotiadis *et al.*, 2024]. Structural connectivity (SC) usually refers to the physical connection between brain regions [Zhang *et al.*, 2024], while functional connectivity (FC) refers to the temporal co-activation between activities in different brain regions [Gao and Wu, 2016]. SC-FC coupling integrates cross-information of structural and functional brain networks and can detect abnormalities more sensitively than relying on either network alone [Ma *et al.*, 2021]. Existing studies have shown that changes in SC-FC coupling are considered potential biomarkers [Popp *et al.*, 2024] and are closely related to the occurrence of a variety of brain diseases, such as schizophrenia, epilepsy, Alzheimer's disease, and Parkinson's Disease, etc [Zhu and Yu, 2025; Sun *et al.*, 2017]. In addition, SC-FC coupling has been shown to be a unique feature of brain organization, which is affected by genetic factors and provides important clues for understanding changes in cognitive function at different developmental stages [Gu *et al.*, 2021].

A variety of methods have been developed over the past decade to quantify SC-FC coupling, including statistical models, biophysical models, and communication models [Zamani Esfahlani *et al.*, 2022; Griffa *et al.*, 2022]. However, the complex relationship between structural and functional connectivity remains elusive, and current state-of-the-art SC-FC coupling methods have not fully considered the neurobiological mechanisms between SC and FC. Specifically, many SC-FC coupling methods primarily focus on finding statisti-

* Corresponding author

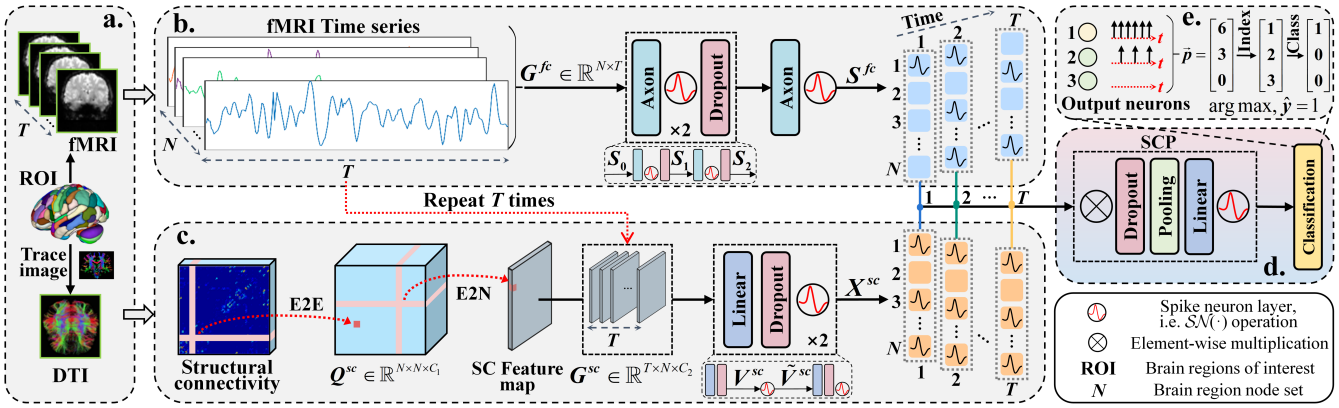

Figure 1: The architecture of the proposed spike-based coupling neural networks (SCNNs) for structural-functional coupling analysis of brain networks. a. Data preprocessing, b. Spike FC feature extraction module, c. Spike SC feature extraction module, d. Spike coupling pooling (SCP), e. Example of output neuron classification.

cal correlations between SC and FC topology patterns, lacking principled system-level integrated to characterize the coupling mechanism of how neuronal populations communicate and generate significant brain function on top of structural connectivity [Dan *et al.*, 2023]. Therefore, to more accurately describe the SC-FC coupling relationship, models more consistent with neurobiological principles must be employed.

To this end, we propose a biologically inspired deep-learning model called spike-based coupling neural networks (SCNNs), which uses spike neurons to characterize the dynamic interaction behavior of SC and FC to understand the SC-FC coupling relationship in the human brain. In addition, to establish the interaction mechanism between SC and FC in the brain, that is, how to accurately quantify SC-FC coupling, we focus on designing a new spike coupling pooling (SCP) module to effectively integrate the interaction between brain structure and function. The schematic diagram of our proposed method is shown in Figure 1. Specifically, we use spike neurons to capture the FC temporal characteristics of the original fMRI time series and the SC spatial characteristics of the structural brain network, and use synaptic and neuronal filter effects to simulate the coupling mechanism of SC and FC in the brain at different temporal and spatial scales. Finally, we fuse SC and FC spike trains through the SCP module to obtain spike SC-FC coupling for brain disease identification. In this work, our contributions are summarized as follows:

- We propose an end-to-end spike train-based framework for analyzing structural and functional relationships, called spike-based coupling neural networks (SCNNs). To the best of our knowledge, the proposed SCNNs are the first deep-learning model that uses spike neurons to understand the SC-FC coupling mechanism from a neurobiological perspective.
- We design a novel low-rank prior-based spike coupling pooling (SCP) module to quantify SC-FC coupling by fusing the variation characteristics of SC in the spatial dimension and the temporal variation of FC in the temporal dimension.
- We evaluate the performance of the proposed method using a real epilepsy dataset, and the results show that the proposed method outperforms existing methods.

2 Method

2.1 Subjects and Data Preprocessing

In this study, we recruited 103 frontal lobe epilepsy (FLE) patients (53 men, 50 women, mean age 24.1), 89 temporal lobe epilepsy (TLE) patients (44 men, 45 women, mean age 25.9), and 114 normal controls (NC) (58 men, 56 women, mean age 26.2). The experiment was approved by the Ethics Committee of Jinling Hospital, Nanjing University Medical School. All subjects provided written informed consent before participation. All subjects were right-handed. The data was collected by a Siemens Trio 3 T magnetic resonance scanner. We used DPARSF and spm12 toolboxes to process the fMRI data, including time correction, alignment, normalization, and detrending and then applied a bandpass filter of 0.01-0.08 Hz. The resulting volume had 240-time points and was divided into 90 regions of interest (ROI) using the automatic anatomical labeling (AAL) atlas. We used PANDA and FSL toolboxes to process Diffusion Tensor Imaging (DTI) data, including distortion correction, extraction of brain masks, deterministic tracking, and definition of anatomical regions based on AAL, with fiber count representing connectivity strength.

2.2 Spiking Neuron Model

The general Leaky Integrate-and-Fire (LIF) neuron [Gerstner and Kistler, 2002] only focuses on the membrane potential dynamics, ignoring synaptic dynamics and SNN filtering, it is difficult to handle the temporal and long-term dependency characteristics in SC and FC. Thus, we use infinite impulse response (IIR) filters to represent the dynamics of LIF neurons [Fang *et al.*, 2021], using their recursive structure to capture the long-term memory effect of the signal and handle the historical dependency and temporal feedback in SC and FC.

We denote the input spike train as a sequence of time-shifted Dirac delta functions: $x_i = \sum_j \delta(t - t_i^j)$, where t_i^j denotes the arrival time of the j_{th} spike from the i_{th} input

synapse. Similarly, the output spike train can be defined as $O(t) = \sum \delta(t - t^f)$, $t^f \in \{t^f : v(t^f) = V_{thre}\}$. Thus, the SNN model is reformulated as a linear constant coefficient difference equation:

$$v[t] = -V_{thre} r[t] + \sum_{i}^{M} \omega_i f_i[t] \tag{1}$$

$$r[t] = e^{\frac{-1}{\tau_r}} r[t-1] + O[t-1] \tag{2}$$

$$O[t] = Hea(v[t] - V_{thre}) \tag{3}$$

$$f_i[t] = \alpha_1 f_i[t-1] + \alpha_2 f_i[t-2] + \beta x_i[t-1] \tag{4}$$

where t is the time, $v[t]$ is the neuron membrane potential, V_{thre} is the threshold potential, ω_i is the associated weight of the i_{th} synapse, M is the total number of synapses, $r[t]$ is the reset filter, τ_r controls the decay speed of the reset impulse, $f_i[t]$ is the second-order IIR filter of the i_{th} synapse, $\alpha_1 = e^{\frac{-1}{\tau_m}} + e^{\frac{-1}{\tau_s}}$, $\alpha_2 = -e^{-\frac{\tau_m + \tau_s}{\tau_m \tau_s}}$, $\beta = e^{\frac{-1}{\tau_m}} - e^{\frac{-1}{\tau_s}}$, τ_m and τ_s are time constants, and $Hea(\cdot)$ is the Heaviside step function, if $x \geq 0$, $Hea(x) = 1$, otherwise $Hea(x) = 0$.

In biological systems, axons often connect multiple target neurons, and their synapses share the same state [Luo, 2021; Shen *et al.*, 2021]. Therefore, tracking the state of synapses with the same neuron is unnecessary, because these synapses can share the same state and computation. Furthermore, the state of neuron $v[t]$ may also depend on past states, which enables SNN to be interpreted as IIR filter networks with nonlinear neurons:

$$V_i^l[t] = \eta V_i^l[t-1] + \sum_{j}^{N_{l-1}} \omega_{i,j}^l F_j^l[t] - V_{thre} R_i^l[t] \tag{5}$$

$$R_i^l[t] = \lambda R_i^l[t-1] + O_i^l[t-1] \tag{6}$$

$$O_i^l[t] = Hea(V_i^l[t] - V_{thre}) \tag{7}$$

$$F_j^l[t] = \sum_{p=1}^{P} \alpha_{j,p}^l F_j^l[t-p] + \sum_{q=0}^{Q} \beta_{j,q}^l O_j^{l-1}[t-q] \tag{8}$$

where i and l represent the index of the neuron and layer respectively, j represents the input index, and N_l is the number of neurons in the l_{th} layer. $V_i^l[t]$ is the neuron membrane potential, $R_i^l[t]$ is the reset voltage, $O_i^l[t]$ is the spike function, and $F_j^l[t]$ is the postsynaptic potential. η and λ are the coefficients of the neuron filter and the reset filter respectively. P and Q represent the feedback and feedforward orders, while $\alpha_{j,p}^l$ and $\beta_{j,q}^l$ are the coefficients of the synaptic filter. We show the SNN model simulated by IIR filters in Figure 2(a). It is worth noting that better to simulate the dynamic behavior of biological neural networks, we use alpha synapses [Ye, 2021] to simulate neuron, where $\alpha_1 = 2e^{-\frac{1}{\tau_r}}$, $\alpha_2 = -e^{-\frac{2}{\tau_r}}$, $\alpha_p = 0$, $p \in \{3, 4, ..., P\}$ and $\beta_1 = \frac{1}{\tau_r} e^{-\frac{1}{\tau_r}}$, $\beta_q = 0$, $q \in \{0, 2, 3, ..., Q\}$.

Let $Axon(\cdot)$ represent the operation of transmitting a spike to the next neuron, which can be simulated by a second-order exponential IIR filter in Eq. 8. Let $\mathcal{SN}(\cdot)$ represent the behavior of the neuron updating the membrane potential and firing

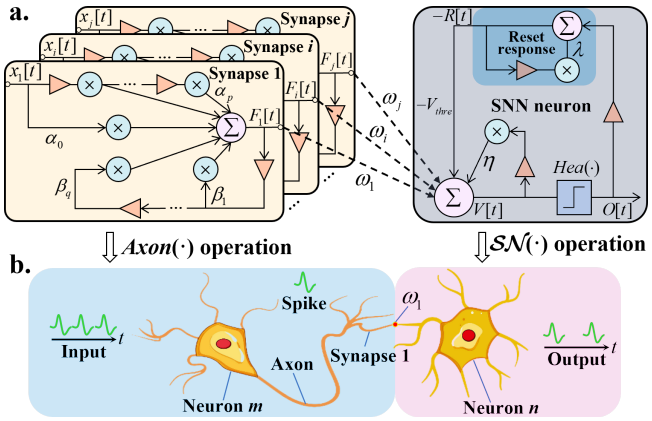

Figure 2: a. SNN model simulated by IIR filter, including two operations: $Axon(\cdot)$ and $\mathcal{SN}(\cdot)$. b. The connection structure composed of two biological neurons shows the neural simulation process of two operations: $Axon(\cdot)$ and $\mathcal{SN}(\cdot)$. For intuitiveness, we assume that the axon of neuron m only contains synapse 1, the corresponding weight is ω_1, and the remaining synapses are negligible.

spikes, as shown in Eq. 5 to 7. Therefore, the SNN model simulated by the IIR filter can be divided into two operations, $Axon(\cdot)$ and $\mathcal{SN}(\cdot)$. For ease of understanding, we provide a specific example in Figure 2(b).

2.3 Spike FC Feature Extraction Module

Based on the advantages of SNN in accurately capturing spike train and temporal patterns [Guo *et al.*, 2023], we adopt a temporal coding method to encode the signal through precise spike timing, effectively representing FC information in the original fMRI time series. In addition, we use the SNN model simulated by IIR filters to capture the time series features in fMRI. Let $G^{fc} \in \mathbb{R}^{N \times T}$ represent the time series matrix of fMRI, N correspond to the set of brain regions nodes, and T correspond to the length of the time series. We use G^{fc} as the functional input of SCNNs and obtain the FC spike matrix through the $Axon(\cdot)$ and $\mathcal{SN}(\cdot)$ operations:

$$S_l = \mathcal{SN}_l(Axon_l(S_{l-1})), \quad l = 1, ..., L \tag{9}$$

where l is the layer index, here $L = 3$. When $l = 1$, $S_{l-1} = G^{fc}$. The final output FC spike matrix is denoted as $S^{fc} \in \mathbb{R}^{N \times T}$. We show the detailed process for calculating the spike FC in Figure 1(b).

2.4 Spike SC Feature Extraction Module

Considering the graph structure of structural connections, this study uses Convolutional Neural Networks for Brain Networks (BrainNetCNN) [Kawahara *et al.*, 2017] to obtain complex features from structural brain network data. Specifically, we use E2E (Edge-to-Edge) and E2N (Edge-to-Node) convolutions to extract features from structural brain networks hierarchically. We will introduce these two convolution operations in detail. Let $A^{sc} \in \mathbb{R}^{|N| \times |N|}$ denote the adjacency matrix of SC and N correspond to the node set of brain regions.

E2E Convolution. E2E convolution is used to extract edge features from the original adjacency matrix. It takes advantage of the topological structure of the network and performs

filtering operations by combining the weights of the edges of shared nodes. Its mathematical form is expressed as follows:

$$Q_{i,j}^{(n)} = f^n(\sum_{k=1}^{|N|} r_d^n A_{i,d}^{sc} + c_d^n A_{d,j}^{sc}) \tag{10}$$

where $r^n \in \mathbb{R}^{|N|}$ and $c^n \in \mathbb{R}^{|N|}$ are the learned weights, f^n represents the nonlinear activation function of the n_{th} filter.

E2N Convolution. E2N convolution aggregates edge features into node features, which extract information from the neighboring edges of each node and generate a representation of each node. Therefore, the output of the E2N layer is defined as:

$$G_i^{(n)} = f^n(\sum_{m=1}^{M}\sum_{k=1}^{|N|} r_d^{m,n} Q_{i,d}^m) \tag{11}$$

where $r_d^{m,n} \in \mathbb{R}^{|N|}$ is the learned weight, (m, n) represents each pair of input and output feature maps of each layer.

The features of SC can be extracted hierarchically through E2E and E2N convolution operations. As shown in Figure 1(c), the SC feature map after the E2E convolution is $Q^{sc} \in \mathbb{R}^{N\times N\times C_1}$, and the feature map after the E2N convolution is $G^{sc} \in \mathbb{R}^{N\times C_2}$, where C_1 and C_2 are the number of filters for the two convolution operations, respectively.

We use the SC feature map G^{sc} after E2E and E2N convolution operations as the structural input of SCNNs and perform implicit spike encoding through internal spike neurons. Figure 1(c) shows the detailed process of calculating spike SC. We obtain the SC spike matrix through the $\mathcal{SN}(\cdot)$ operation and the linear network:

$$\tilde{V}^{sc} = \mathcal{SN}(V^{sc}), \quad V^{sc} \in \mathbb{R}^{T\times N\times D} \tag{12}$$

$$X^{sc} = \mathcal{SN}(Linear(\tilde{V}^{sc})), \quad X^{sc} \in \mathbb{R}^{N\times T} \tag{13}$$

where X^{sc} is the final output SC spike matrix, D is the feature dimension and T is the time step. It is worth noting that the choice of T is determined by the length of the fMRI time series. V^{sc} is obtained by passing G^{sc} through a linear network after T repetitions. $\tilde{V}^{sc}$ is obtained by passing it through $\mathcal{SN}(\cdot)$, so it is a binary spike tensor.

2.5 Spike Coupling Pooling Module

After the above operations, we obtain the FC spike matrix S^{fc} and SC spike matrix X^{sc} containing the functional and structural information of the brain network. Since S^{fc} and X^{sc} are high-dimensional binary spike signals, direct calculation may lead to increased memory cost and the risk of overfitting [Yu *et al.*, 2017]. Thus, we propose a spike coupling pooling (SCP) module based on a low-rank prior to effectively quantify the coupling relationship between FC and SC by low-rank decomposition, thereby reducing the amount of computation and improving model efficiency.

The functional and structural inputs of SCP can be described as $S^{fc} = (s_0, ..., s_t, ..., s_T)$, $s_t \in \mathbb{R}^N$ and $X^{sc} = (x_0, ..., x_t, ..., x_T)$, $x_t \in \mathbb{R}^N$ respectively. For ease of explanation, we focus on the processing at time t ($t \in [0, T]$). Specifically, given the FC feature vector s_t and the SC feature vector x_t at time t, the simplest bilinear transformation is defined as $h_t = s_t^{(tr)} W x_t \in \mathbb{R}$, where $W \in \mathbb{R}^{N\times N}$ is the projection matrix, (tr) represents the transpose operator. To obtain a o-dimensional output, we need to learn $W \in \mathbb{R}^{N\times N\times o}$, which results in a large number of parameters. However, W can be factorized into two low-rank matrices:

$$h_t = s_t^{(tr)} P Q^{(tr)} x_t = \mathbf{1}^{(tr)}(P^{(tr)} s_t \otimes Q^{(tr)} x_t) \tag{14}$$

where k is the factorization rank, $\otimes$ is the element-wise multiplication (Hadamard) of two eigenvectors, $\mathbf{1} \in \mathbb{R}^k$ is an all-ones vector, $P \in \mathbb{R}^{N\times k}$, $Q \in \mathbb{R}^{N\times k}$. Therefore, to obtain an output feature vector $h_t \in \mathbb{R}^o$, two 3-D tensors $\tilde{P} = [P_1, P_2, ..., P_o] \in \mathbb{R}^{N\times k\times o}$ and $\tilde{Q} = [Q_1, Q_2, ..., Q_o] \in \mathbb{R}^{N\times k\times o}$ are required. Without loss of generality, we can reformulate $\tilde{P}$ and $\tilde{Q}$ as 2-D matrices $P' \in \mathbb{R}^{N\times ko}$ and $Q' \in \mathbb{R}^{N\times ko}$ respectively with simple reshape operation. The final fused vector $h_t^{sc-fc} \in \mathbb{R}^o$ is obtained by performing sum pooling on the projection vectors using P' and Q' with a 1-D non-overlapping window of size k:

$$h_t^{sc-fc} = \text{SumPool}(P'^{(tr)} s_t \otimes Q'^{(tr)} x_t, k) \tag{15}$$

As shown in Figure 1(d) and Figure 3, the above operation generates a feature vector h_t^{sc-fc} that combines FC temporal information and SC spatial information. It only represents the coupling relationship between FC and SC at time t. After repeating the above operation T times, we obtain a spike matrix $H^{sc-fc} \in \mathbb{R}^{T\times o}$ consisting of T feature vectors, which we call spike SC-FC coupling. It not only contains temporal FC features, but also retains spatial SC features, and fully characterizes the coupling relationship between FC and SC. Finally, we can get the spike $\vec{Z}[t] \in \mathbb{R}^m$ fired by each output neuron over time through the linear network and $\mathcal{SN}(\cdot)$ operation. It is a vector that changes over time, where m is the number of output classes.

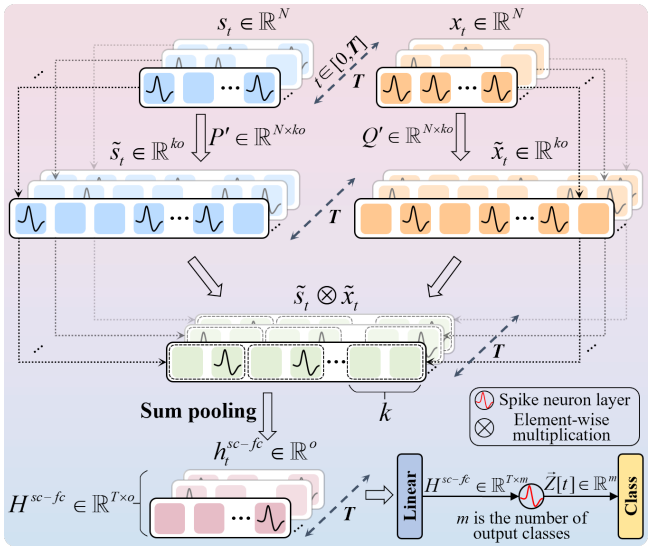

Figure 3: Details of spike coupling pooling (SCP) module.

Method	FLE vs. NC						TLE vs. NC					
	ACC	SEN	SPE	PPV	NPV	BAC	ACC	SEN	SPE	PPV	NPV	BAC
Statistic [Chiang *et al.*, 2015]	68.18	57.14	78.26	70.59	66.67	67.70	65.91	61.90	69.57	65.00	66.67	65.73
Multi-kernel [Dyrba *et al.*, 2015]	74.57	63.86	84.44	79.10	71.10	74.15	73.17	61.11	82.61	73.33	73.08	71.86
MPCA [Huang *et al.*, 2020]	76.30	71.08	81.11	77.63	75.26	76.10	77.46	75.90	78.89	76.83	78.02	77.40
Self-calibrated [Lei *et al.*, 2020]	77.16	74.32	79.55	75.34	78.65	76.93	76.15	70.15	82.54	81.03	72.22	76.34
C-BSF [Liu *et al.*, 2024]	79.23	80.56	77.59	81.69	76.27	79.07	76.92	76.39	77.59	80.88	72.58	76.99
DCNN [Atwood and Towsley, 2016]	80.77	72.22	91.38	91.23	72.60	81.80	79.77	72.22	87.95	86.67	74.49	80.09
MVGCN [Zhang *et al.*, 2018]	81.54	79.17	84.48	86.36	76.56	81.82	83.08	77.78	89.66	90.32	76.47	83.72
Brain-DNN [Sarwar *et al.*, 2021]	82.72	75.68	88.64	84.85	81.25	82.16	82.10	68.92	93.18	89.47	78.10	81.05
Brain-GRL [Li *et al.*, 2022]	83.33	71.62	93.18	89.83	79.61	82.40	84.57	76.47	90.43	85.25	84.16	83.45
MMP-GCN [Song *et al.*, 2022]	85.80	74.32	95.45	93.22	81.55	84.89	85.19	74.63	92.63	87.72	83.81	83.63
Brain-GCN [Xia *et al.*, 2024]	88.73	81.54	94.81	92.98	85.88	88.17	85.21	81.54	88.31	85.48	85.00	84.93
SFDN [Wei *et al.*, 2024a]	87.65	78.38	95.45	93.55	84.00	86.92	87.69	85.71	89.55	88.52	86.96	87.63
Kuramoto [Dan *et al.*, 2023]	89.51	81.08	**96.59**	95.24	85.86	88.84	90.12	85.14	94.32	92.65	88.30	89.73
Koopman [Chow *et al.*, 2024]	90.29	89.29	91.30	92.59	87.50	90.30	91.67	94.12	89.86	87.27	95.38	91.99
NeuroPath [Wei *et al.*, 2024b]	93.33	91.07	95.31	94.44	92.42	93.19	92.25	**94.74**	90.59	87.10	**96.25**	92.66
SCNNs (Our method)	**95.16**	**94.12**	96.43	**96.97**	**93.10**	**95.27**	**94.17**	92.59	**95.45**	**94.34**	94.03	**94.02**

Table 1: Test accuracy (%) comparison of different methods. There are three types of methods from top to bottom in the table: i) Based on classifier, ii) Based on DL and iii) Based on DL and neuroscience. All results are averaged over 5 runs. The best results are boldfaced.

2.6 Implementation

Let $\vec{p} \in \mathbb{R}^m$ count the spikes of each output neuron, which can be obtained by summing $\vec{Z}[t]$ over T time steps:

$$\vec{p} = \sum_{t=0}^{T} \vec{Z}[t] \tag{16}$$

The index of $\vec{p}$ with the maximum count corresponds to the predicted class $\hat{y}$:

$$\hat{y} = \arg\max_j p_j \tag{17}$$

We provide an example in Figure 1(e), where neuron 1 fired 6 spikes, neuron 2 fired 3 spikes, and neuron 3 fired no spikes. Compared to neurons 2 and 3, neuron 1 has the maximum spike count, and the corresponding prediction class is 1. In addition, to train the SCNNs architecture, we use the classification cross-entropy loss function L_c. For binary classification tasks, the cross-entropy loss is calculated as follows:

$$L_c = -(\hat{y} \log \hat{y} + (1 - \hat{y}) \log(1 - y)) \tag{18}$$

where y is the true label.

3 Experiments and Results

3.1 Experimental Setup

The proposed model and algorithm are implemented in PyTorch and snnTorch [Eshraghian *et al.*, 2023], and the GPU used in training is NVIDIA RTX 4090. We first briefly introduce the architecture of BrainNetCNN. The input of the BrainNetCNN model is the structural brain network A^{sc}, represented as a 90×90 adjacency matrix. In our experiment, the E2E layer is composed of [32, 1×90] and [32, 90×1] filters producing feature maps of size $90 \times 90 \times 32$. Next is the E2N layer, composed of [64, $1 \times 90 \times 32$] filters producing SC feature maps of size $1 \times 90 \times 64$. For the design of SCNNs, we employ synapse model depicted by Eq. 8, in which $\tau_r = 0.9$, $V_{thre} = 1$, $\eta = 1$, $\lambda = e^{-\frac{1}{\tau_r}}$, $T = 240$. During training, we use a dropout of 0.1 and use the Adam optimizer with hyperparameters $\theta_1 = 0.9$ and $\theta_2 = 0.999$. The learning rate is 1×10^{-3}, the training epochs are 100, factorization rank $k = 3$.

We mainly perform two binary classification tasks: FLE vs. NC and TLE vs. NC task. The performance of our method is evaluated with the following metrics: accuracy (ACC $= \frac{\text{TP+TN}}{\text{TP+TN+FP+FN}}$), sensitivity (SEN $= \frac{\text{TP}}{\text{TP+FN}}$), specificity (SPE $= \frac{\text{TN}}{\text{TN+FP}}$), positive predictive value (PPV $= \frac{\text{TP}}{\text{TP+FP}}$), negative predictive value (NPV $= \frac{\text{TN}}{\text{TN+FN}}$), and balanced accuracy (BAC $= \frac{\text{SEN+SPE}}{2}$). FP, TP, FN and TN represent false-positive, true-positive, false-negative, and true-negative classification results. It is worth noting that the selection of parameters and other experiments are performed using a five-fold cross-validation strategy.

3.2 Methods for Comparison

To verify the effectiveness of the SCNNs method, we compare SCNNs with existing SC-FC coupling analysis methods. For convenience, we divide the comparison methods into three types and briefly introduce the basic characteristics of these three types of comparison methods below.

The first type is the traditional SC-FC coupling methods based on classifiers, mainly including i) Direct statistics (**Statistics**) [Chiang *et al.*, 2015], ii) Multi-kernel learning method (**Multi-kernel**) [Dyrba *et al.*, 2015], iii) Multilinear principal component analysis (**MPCA**) [Huang *et al.*, 2020], iv) **Self-calibrated** [Lei *et al.*, 2020] and v) Coupling in Brain SC and FC (**C-BSF**) [Liu *et al.*, 2024]. These methods focus on modeling and analyzing SC-FC coupling using statistics and classical machine learning algorithms, usually relying on feature extraction and selection, combined with support vector machines, random forests, and other machine learning classifiers for prediction and classification.

The second type is methods based on deep learning (DL),

mainly including i) Diffusion-convolutional neural networks (**DCNN**) [Atwood and Towsley, 2016], ii) Multi-view graph convolutional network (**MVGCN**) [Zhang *et al.*, 2018], iii) Deep neural network (**BrainDNN**) [Sarwar *et al.*, 2021], iv) Supervised graph representation learning (**Brain-GRL**) [Li *et al.*, 2022], v) Multicenter and multichannel pooling graph convolutional network (**MMP-GCN**) [Song *et al.*, 2022], vi) Graph convolutional network (**Brain-GCN**) [Xia *et al.*, 2024] and vii) SC-FC detour network (**SFDN**) [Wei *et al.*, 2024a]. These methods use deep neural networks to extract complex features in brain network data, and gradually extract higher-level features through a multi-level network structure, thereby improving the prediction accuracy of the model.

The third type is to introduce neuroscience improvement methods into DL methods, mainly including i) Deep **Kuramoto** model [Dan *et al.*, 2023], ii) Neural **Koopman** operator [Chow *et al.*, 2024] and iii) Neural pathway transformer (**NeuroPath**) [Wei *et al.*, 2024b]. These methods combine neurobiological mechanisms and improve the neural network structure by simulating the activity and connection mode of brain neurons, so as to better capture biological characteristics and laws. This type of method has certain similarities with the SCNNs we proposed in terms of ideas, and both try to improve the performance of DL models by drawing inspiration from neuroscience.

3.3 Classification Performance

The experimental performance of each method in the FLE vs. NC and TLE vs. NC tasks is shown in Table 1. Specifically, the ACC of the SCNNs method proposed by us for epilepsy identification reaches 95.16% and 94.17% in two tasks, respectively. In comparison, only the third type of method (Based on DL and neuroscience) has an ACC of more than 90%, while the first type of method (Based on classifier) and the second type of method (Based on DL) do not reach 90%. By introducing neuroscience and biological mechanisms, the disease prediction accuracy of the model is significantly improved, and SCNNs perform best among these methods.

From the perspective of other evaluation indicators, in the FLE vs. NC task, the SEN of the SCNNs method is 3.05% higher than that of the best NeuroPath method among other methods. Similarly, in the three indicators of PPV, NPV, and BAC, the SCNNs method shows improvements of 0.68% to 2.08%. In addition, the SPE of the Kuramoto method is slightly higher than that of SCNNs, with a difference of 0.16%, while the SPE values of other methods are lower than that of SCNNs. In the TLE vs. NC task, although the NeuroPath method outperforms SCNNs in the SPE and NPV indicators, the SCNNs method performs best in SPE, PPV, and BAC. Overall, the comprehensive performance of our proposed SCNNs method in identifying epilepsy is significantly better than that of other methods.

3.4 Spike SC-FC Coupling Statistical Analysis

To demonstrate the effectiveness of the SC-FC coupling features obtained by our method, we performed statistical analysis. Specifically, in the experiment, we count the total number of spike SC-FC couplings fired in 90 brain regions of FLE, TLE patients, and normal controls in the test sets of the two

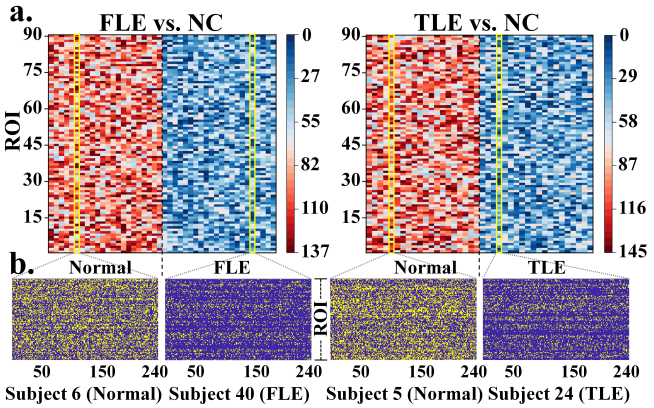

Figure 4: a. Total number of spike SC-FC couplings fired in 90 brain regions in FLE, TLE patients, and normal controls in the test sets of the FLE vs. NC and TLE vs. NC tasks. The horizontal axis represents each subject. b. Spike SC-FC coupling generated by a single subject in both tasks, presented as spike raster plots. Each yellow bar represents the firing of a neuron.

tasks. For ease of observation, we show in Figure 4 the total number of spike SC-FC couplings fired in 90 brain regions in the test set in the FLE vs. NC and TLE vs. NC tasks, as well as the visualization results of the spike SC-FC couplings generated by a single subject. It is clear from Figure 4 that, within 240 time points, almost every brain region of normal controls fires a large number of spikes, while some brain regions of FLE and TLE patients do not fire spikes, and other brain regions only fire a small number of spikes. We speculate that epilepsy disrupts information transmission and cognitive circuits within the brain, interfering with normal communication between brain regions. Abnormal electrical activity may also cause damage to neurons, thereby affecting the normal performance of spike SC-FC coupling.

To further verify the reliability of the results, we perform a statistical analysis on the total number of spike SC-FC couplings fired by patients and normal controls across 90 brain regions in the two tasks of FLE vs. NC and TLE vs. NC. The results show that the difference between patients and normal controls is statistically significant. We present the five brain regions with the most significant differences and their box plots in Figure 5. It is clearly visible from Figure 5 that the number of spike SC-FC couplings fired by normal controls in these five brain regions is large and densely distributed, while the spike SC-FC couplings fired by FLE and TLE patients in these regions are significantly fewer and more sparsely distributed. Some previous studies have also confirmed similar findings, although these studies mainly focus on traditional SC-FC coupling rather than SC-FC coupling in the form of spike trains. For example, [Sinha *et al.*, 2023] and [Zhou *et al.*, 2024] report that, compared with normal controls, the SC-FC coupling in certain brain regions of epileptic patients exhibits weaker responses or inactive states. [Shah *et al.*, 2019] and [Wang *et al.*, 2015] point out that SC-FC coupling in patients with epilepsy is significantly reduced compared with normal controls, particularly during epileptic seizures, where the reduction trend becomes even more pronounced. These

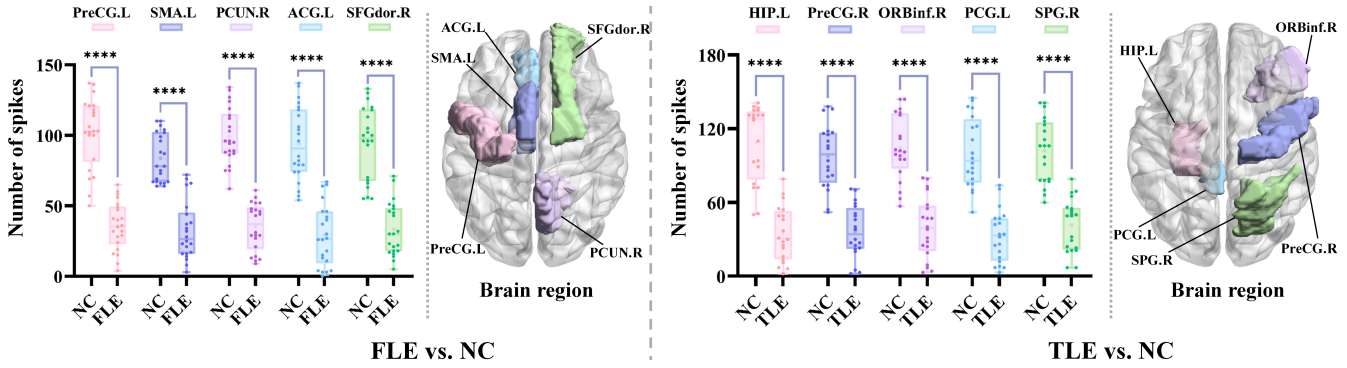

Figure 5: Statistical analysis of the total spike SC-FC couplings and brain region activation in the FLE vs. NC and TLE vs. NC tasks. Here, only the distribution and boxplots of the 5 most significantly different brain regions are shown. The cross in the middle of each boxplot indicates the average value, $**$ represents $p < 0.0001$, and $p < 0.05$ is considered significant. (PreCG: Precentral, SMA: Supp Motor Area, PCUN: Precuneus, ACG: Cingulum Ant, SFGdor: Frontal Sup, HIP: Hippocampus, ORBinf: Frontal Inf Orb, PCG: Cingulum Post, SPG: Parietal Sup).

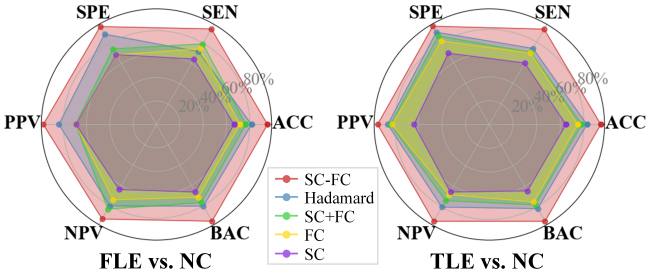

Figure 6: Radar chart to verify the effectiveness of SCP module.

findings are consistent with our current results, which show that the reduction in SC-FC coupling corresponds to a decrease in the number of spike SC-FC couplings fired. Additionally, the brain regions with significant differences (such as PreCG.L, SMA.L, and ACG.L in the FLE vs. NC task, as well as HIP.L and PCG.L in the TLE vs. NC task) are also shown to be associated with frontal lobe [O'Muircheartaigh and Richardson, 2012] and temporal lobe epilepsy [Pitkänen and Sutula, 2002]. These results further demonstrate that epileptic seizures are closely linked to impaired connectivity and abnormal electrical activity patterns between brain regions, thereby confirming the reliability of our findings.

3.5 Spike Coupling Pooling Module Validity

To verify the effectiveness of the spike coupling pooling (SCP) module in SCNNs, we conduct ablation experiments on the same dataset. Specifically, we design the following three multimodal fusion and two single-modal comparison methods: i) **SC-FC**: retain the SCP module without any changes, ii) **Hadamard**: remove the low-rank decomposition and pooling operations in the SCP module, and only use the Hadamard product to calculate the spike SC-FC coupling, iii) **SC+FC**: concatenate and fuse the spike FC and SC and input them into the classification layer to obtain accuracy, iv) **FC**: train SCNNs using only single-modal FC (original fMRI time series), v) **SC**: train SCNNs using only single-modal SC.

The results are shown in the radar chart of Figure 6, we find that in both tasks, the multimodal fusion method consistently outperforms the single-modal method, and the SC-FC method with the SCP module retained achieves the best performance among the multimodal fusion methods. Specifically, in the FLE vs. NC task, the ACC of the single-modal methods, FC and SC, is 71.54% and 66.47%, respectively. In the multimodal methods, the ACC of Hadamard and SC+FC is 81.48% and 76.54%, respectively, both significantly better than the single-modal methods. However, the ACC of the SC-FC method reaches 95.16%, outperforming both Hadamard and SC+FC. Similarly, in the TLE vs. NC task, the SC-FC method with the SCP module retained also demonstrates a clear advantage. In addition, we find that the performance of single-modal FC is slightly better than that of single-modal SC, which may be because the original fMRI time series contains more dynamic information related to epilepsy, making FC more prominent in extracting effective features. These results indicate that both FC and SC are indispensable, and that the spike SC-FC coupling generated by the fusion of the two comprehensively considers structural and functional information and can more accurately capture the dynamic characteristics of brain networks.

4 Conclusion

This study proposes spike-based coupling neural networks (SCNNs) for understanding the SC-FC coupling relationship in the human brain, which simulates the interaction of SC and FC in the brain through dense interconnection of spiking neurons and synaptic weights, and quantifies SC-FC coupling using spike timing and network activity characteristics. Our experiments on a real epilepsy dataset demonstrate the superior performance of SCNNs in brain disease diagnosis and provide a new perspective for SC-FC coupling analysis.

Acknowledgments

This study was supported in part by the National Natural Science Foundation of China (No. 62471259, 62472228, 62406153, 62376123), and the Natural Science Founda-

tion of Jiangsu Higher Education Institutions of China (No. 24KJB520032, 23KJB520031).

Contribution Statement

Shaolong Wei and Shu Jiang contributed equally to this work.

References

[Anderson and Finlay, 2014] Michael L Anderson and Barbara L Finlay. Allocating structure to function: the strong links between neuroplasticity and natural selection. *Frontiers in human neuroscience*, 7:918, 2014.

[Atwood and Towsley, 2016] James Atwood and Don Towsley. Diffusion-convolutional neural networks. *Advances in neural information processing systems*, 29, 2016.

[Chiang *et al.*, 2015] Sharon Chiang, John M Stern, Jerome Engel Jr, and Zulfi Haneef. Structural–functional coupling changes in temporal lobe epilepsy. *Brain research*, 1616:45–57, 2015.

[Chow *et al.*, 2024] Chiyuen Chow, Tingting Dan, Martin Styner, and Guorong Wu. Understanding brain dynamics through neural koopman operator with structure-function coupling. In *International Conference on Medical Image Computing and Computer-Assisted Intervention*, pages 509–518. Springer, 2024.

[Dan *et al.*, 2023] Tingting Dan, Minjeong Kim, Won Hwa Kim, and Guorong Wu. Uncovering structural-functional coupling alterations for neurodegenerative diseases. In *International Conference on Medical Image Computing and Computer-Assisted Intervention*, pages 87–96. Springer, 2023.

[Dyrba *et al.*, 2015] Martin Dyrba, Michel Grothe, Thomas Kirste, and Stefan J Teipel. Multimodal analysis of functional and structural disconnection in a lzheimer's disease using multiple kernel svm. *Human brain mapping*, 36(6):2118–2131, 2015.

[Eshraghian *et al.*, 2023] Jason K Eshraghian, Max Ward, Emre O Neftci, Xinxin Wang, Gregor Lenz, Girish Dwivedi, Mohammed Bennamoun, Doo Seok Jeong, and Wei D Lu. Training spiking neural networks using lessons from deep learning. *Proceedings of the IEEE*, 2023.

[Fang *et al.*, 2021] Haowen Fang, Amar Shrestha, Ziyi Zhao, and Qinru Qiu. Exploiting neuron and synapse filter dynamics in spatial temporal learning of deep spiking neural network. In *Proceedings of the Twenty-Ninth International Conference on International Joint Conferences on Artificial Intelligence*, pages 2799–2806, 2021.

[Fotiadis *et al.*, 2024] Panagiotis Fotiadis, Linden Parkes, Kathryn A Davis, Theodore D Satterthwaite, Russell T Shinohara, and Dani S Bassett. Structure–function coupling in macroscale human brain networks. *Nature Reviews Neuroscience*, 25(10):688–704, 2024.

[Gao and Wu, 2016] Lin-lin Gao and Tao Wu. The study of brain functional connectivity in parkinson's disease. *Translational neurodegeneration*, 5:1–7, 2016.

[Gerstner and Kistler, 2002] Wulfram Gerstner and Werner M Kistler. *Spiking neuron models: Single neurons, populations, plasticity*. Cambridge university press, 2002.

[Griffa *et al.*, 2022] Alessandra Griffa, Enrico Amico, Raphaël Liégeois, Dimitri Van De Ville, and Maria Giulia Preti. Brain structure-function coupling provides signatures for task decoding and individual fingerprinting. *NeuroImage*, 250:118970, 2022.

[Gu *et al.*, 2021] Zijin Gu, Keith Wakefield Jamison, Mert Rory Sabuncu, and Amy Kuceyeski. Heritability and interindividual variability of regional structure-function coupling. *Nature Communications*, 12(1):4894, 2021.

[Guo *et al.*, 2023] Lei Guo, Minxin Guo, Youxi Wu, and Guizhi Xu. Specific neural coding of fmri spiking neural network based on time coding. *Chaos, Solitons & Fractals*, 174:113821, 2023.

[Huang *et al.*, 2020] Jiashuang Huang, Luping Zhou, Lei Wang, and Daoqiang Zhang. Attention-diffusion-bilinear neural network for brain network analysis. *IEEE transactions on medical imaging*, 39(7):2541–2552, 2020.

[Kanwisher *et al.*, 2023] Nancy Kanwisher, Meenakshi Khosla, and Katharina Dobs. Using artificial neural networks to ask 'why'questions of minds and brains. *Trends in Neurosciences*, 46(3):240–254, 2023.

[Kawahara *et al.*, 2017] Jeremy Kawahara, Colin J Brown, Steven P Miller, Brian G Booth, Vann Chau, Ruth E Grunau, Jill G Zwicker, and Ghassan Hamarneh. Brainnetcnn: Convolutional neural networks for brain networks; towards predicting neurodevelopment. *NeuroImage*, 146:1038–1049, 2017.

[Lei *et al.*, 2020] Baiying Lei, Nina Cheng, Alejandro F Frangi, Ee-Leng Tan, Jiuwen Cao, Peng Yang, Ahmed Elazab, Jie Du, Yanwu Xu, and Tianfu Wang. Self-calibrated brain network estimation and joint non-convex multi-task learning for identification of early alzheimer's disease. *Medical image analysis*, 61:101652, 2020.

[Li *et al.*, 2022] Yang Li, Gonzalo Mateos, and Zhengwu Zhang. Learning to model the relationship between brain structural and functional connectomes. *IEEE Transactions on Signal and Information Processing over Networks*, 8:830–843, 2022.

[Liu *et al.*, 2024] Chang Liu, Jing Jing, Jiyang Jiang, Wei Wen, Wanlin Zhu, Zixiao Li, Yuesong Pan, Xueli Cai, Hao Liu, Yijun Zhou, et al. Relationships between brain structure-function coupling in normal aging and cognition: A cross-ethnicity population-based study. *NeuroImage*, 299:120847, 2024.

[Luo, 2021] Liqun Luo. Architectures of neuronal circuits. *Science*, 373(6559):eabg7285, 2021.

[Ma *et al.*, 2021] Juanwei Ma, Feng Liu, Bingbing Yang, Kaizhong Xue, Pinxiao Wang, Jian Zhou, Yang Wang, Yali Niu, and Jing Zhang. Selective aberrant functional–structural coupling of multiscale brain networks in subcortical vascular mild cognitive impairment. *Neuroscience Bulletin*, 37:287–297, 2021.

[O'Muircheartaigh and Richardson, 2012] Jonathan O'Muircheartaigh and Mark P Richardson. Epilepsy and the frontal lobes. *Cortex*, 48(2):144–155, 2012.

[Park and Friston, 2013] Hae-Jeong Park and Karl Friston. Structural and functional brain networks: from connections to cognition. *Science*, 342(6158):1238411, 2013.

[Pessoa, 2014] Luiz Pessoa. Understanding brain networks and brain organization. *Physics of life reviews*, 11(3):400–435, 2014.

[Petersen and Sporns, 2015] Steven E Petersen and Olaf Sporns. Brain networks and cognitive architectures. *Neuron*, 88(1):207–219, 2015.

[Pitkänen and Sutula, 2002] Asla Pitkänen and Thomas P Sutula. Is epilepsy a progressive disorder? prospects for new therapeutic approaches in temporal-lobe epilepsy. *The Lancet Neurology*, 1(3):173–181, 2002.

[Popp *et al.*, 2024] Johanna L Popp, Jonas A Thiele, Joshua Faskowitz, Caio Seguin, Olaf Sporns, and Kirsten Hilger. Structural-functional brain network coupling predicts human cognitive ability. *NeuroImage*, 290:120563, 2024.

[Sarwar *et al.*, 2021] Tabinda Sarwar, Ye Tian, BT Thomas Yeo, Kotagiri Ramamohanarao, and Andrew Zalesky. Structure-function coupling in the human connectome: A machine learning approach. *NeuroImage*, 226:117609, 2021.

[Shah *et al.*, 2019] Preya Shah, Arian Ashourvan, Fadi Mikhail, Adam Pines, Lohith Kini, Kelly Oechsel, Sandhitsu R Das, Joel M Stein, Russell T Shinohara, Danielle S Bassett, et al. Characterizing the role of the structural connectome in seizure dynamics. *Brain*, 142(7):1955–1972, 2019.

[Shen *et al.*, 2021] Jiangrong Shen, Yu Zhao, Jian K Liu, and Yueming Wang. Hybridsnn: Combining bio-machine strengths by boosting adaptive spiking neural networks. *IEEE Transactions on Neural Networks and Learning Systems*, 34(9):5841–5855, 2021.

[Sinha *et al.*, 2023] Nishant Sinha, John S Duncan, Beate Diehl, Fahmida A Chowdhury, Jane De Tisi, Anna Miserocchi, Andrew William McEvoy, Kathryn A Davis, Sjoerd B Vos, Gavin P Winston, et al. Intracranial eeg structure-function coupling and seizure outcomes after epilepsy surgery. *Neurology*, 101(13):e1293–e1306, 2023.

[Song *et al.*, 2022] Xuegang Song, Feng Zhou, Alejandro F Frangi, Jiuwen Cao, Xiaohua Xiao, Yi Lei, Tianfu Wang, and Baiying Lei. Multicenter and multichannel pooling gcn for early ad diagnosis based on dual-modality fused brain network. *IEEE Transactions on Medical Imaging*, 42(2):354–367, 2022.

[Sporns, 2013] Olaf Sporns. Structure and function of complex brain networks. *Dialogues in clinical neuroscience*, 15(3):247–262, 2013.

[Sun *et al.*, 2017] Yu Sun, Zhongxiang Dai, Junhua Li, Simon L Collinson, and Kang Sim. Modular-level alterations of structure–function coupling in schizophrenia connectome. *Human brain mapping*, 38(4):2008–2025, 2017.

[Wang *et al.*, 2015] Zhijiang Wang, Zhengjia Dai, Gaolang Gong, Changsong Zhou, and Yong He. Understanding structural-functional relationships in the human brain: a large-scale network perspective. *The Neuroscientist*, 21(3):290–305, 2015.

[Wei *et al.*, 2024a] Ziquan Wei, Tingting Dan, Jiaqi Ding, Paul Laurienti, and Guorong Wu. Representing functional connectivity with structural detour: A new perspective to decipher structure-function coupling mechanism. In *International Conference on Medical Image Computing and Computer-Assisted Intervention*, pages 367–377. Springer, 2024.

[Wei *et al.*, 2024b] Ziquan Wei, Tingting Dan, Jiaqi Ding, and Guorong Wu. Neuropath: A neural pathway transformer for joining the dots of human connectomes. *arXiv preprint arXiv:2409.17510*, 2024.

[Xia *et al.*, 2024] Jing Xia, Yi Hao Chan, Deepank Girish, and Jagath C Rajapakse. Brain structure-function interaction network for fluid cognition prediction. In *ICASSP 2024-2024 IEEE International Conference on Acoustics, Speech and Signal Processing (ICASSP)*, pages 1706–1710. IEEE, 2024.

[Ye, 2021] Weijie Ye. Dynamics of a large-scale spiking neural network with quadratic integrate-and-fire neurons. *Neural Plasticity*, 2021(1):6623926, 2021.

[Yu *et al.*, 2017] Zhou Yu, Jun Yu, Jianping Fan, and Dacheng Tao. Multi-modal factorized bilinear pooling with co-attention learning for visual question answering. In *Proceedings of the IEEE international conference on computer vision*, pages 1821–1830, 2017.

[Zamani Esfahlani *et al.*, 2022] Farnaz Zamani Esfahlani, Joshua Faskowitz, Jonah Slack, Bratislav Mišić, and Richard F Betzel. Local structure-function relationships in human brain networks across the lifespan. *Nature communications*, 13(1):2053, 2022.

[Zhang *et al.*, 2018] Xi Zhang, Lifang He, Kun Chen, Yuan Luo, Jiayu Zhou, and Fei Wang. Multi-view graph convolutional network and its applications on neuroimage analysis for parkinson's disease. In *AMIA Annual Symposium Proceedings*, volume 2018, page 1147. American Medical Informatics Association, 2018.

[Zhang *et al.*, 2024] Hui Zhang, Peng Cao, Henry KF Mak, and Edward S Hui. The structural–functional-connectivity coupling of the aging brain. *GeroScience*, pages 1–13, 2024.

[Zhou *et al.*, 2024] Chunyao Zhou, Fangfang Xie, Dongcui Wang, Xiaoting Huang, Danni Guo, Yangsa Du, Ling Xiao, Dingyang Liu, Bo Xiao, Zhiquan Yang, et al. Preoperative structural–functional coupling at the default mode network predicts surgical outcomes of temporal lobe epilepsy. *Epilepsia*, 65(4):1115–1127, 2024.

[Zhu and Yu, 2025] Jiajia Zhu and Yongqiang Yu. Measuring brain structure-function coupling: A promising approach to decode psychiatric neuropathology. *Biological Psychiatry*, 97(3):212–214, 2025.